




The Impact of Altering an Aspect Ratio on the Instabilities of Flow Boiling Characteristics in a Rectangular Microchannel



Shahid M. Talib^{1,2*}, Ekhlas M. Fayyadh², Moayed R. Hasan²

¹ General Directorate for Vocational Education, Ministry of Education, Karbala 56001, Iraq

² Department of Mechanical Engineering, College of Engineering, University of Technology, Baghdad 10066, Iraq

Corresponding Author Email: me.20.18@grad.uotechnology.edu.iq

Copyright: ©2024 The authors. This article is published by IETA and is licensed under the CC BY 4.0 license (<http://creativecommons.org/licenses/by/4.0/>).

<https://doi.org/10.18280/i2m.230608>

ABSTRACT

Received: 23 May 2024

Revised: 22 August 2024

Accepted: 14 October 2024

Available online: 24 December 2024

Keywords:

aspect ratio, flow boiling, microchannel, thermal performance

This study varied the aspect ratio of a single microchannel to analyze fluid flow and heat transmission. The tests used a 0.7-mm-wide, 0.3-mm-deep, 60-mm-long micro-channel. The input temperature was 30°C and deionized water was used. Reynolds numbers examined were 166-2550. The fanning friction factor's link with laminar and turbulent flow can reliably predict experimental outcomes, according to calculations and tests. The Nusselt number also rises with the Reynolds number. Increased aspect ratios improve heat transfer at all Reynolds numbers. Under high mass flow circumstances, increasing aspect ratio from 0.42 to 2.4 reduced wall superheat by 22.7%. At high heat flux, a mass flow rate of 450 kg/m² improves heat transfer coefficient more than 250 kg/m². The biggest improvements are 6.13% and 4.08%. The study shows a correlation between wall heat flow and pressure drop. Inversely, aspect ratio decreases pressure drop. With increasing aspect ratio, nucleate boiling was delayed. As mass flux increased, pressure drop oscillations decreased. Pressure drops oscillate at 2.5 and 2.6 kilopascals for aspect ratios of 0.42 and 2.4.

1. INTRODUCTION

Over the last 30 years, electronic components have steadily downsized, making more reliable thermal management solutions necessary to maintain system temperatures within material and performance concentrates. The origin of this phenomenon may be traced back to about 1980 when there was a rise in heat dissipation. Accordingly, fans for cooling heat sink attachments will be changed to liquid cooling systems. Initially, a liquid solution was exclusively used to cool a flow with a single phase [1].

Karayannis and Mahmoud [2] previously discussed the ongoing essential investigation features and problems that are accountable for this deficiency. An experimental element refers to the influence of tube design. To be more specific, the aspect ratio of the cross-section of rectangular microchannels may impact the flow patterns, heat transfer mechanisms, heat transfer speeds, and pressure variations. Diaz and Schmidt [3] performed an empirical investigation to analyze the heat transfer during water and ethanol flow boiling in a rectangular microchannel with a cross-section of 0.3 mm × 12.7 mm. The experiment demonstrated that the heat transfer coefficient decreased as water quality increased, indicating the prevalence of nucleate boiling in the poor-quality region. Different researches are performed for studying the impact of channel configuration on the properties of heat transfer as well as the reduction of pressure that happens through flow boiling in microchannels. According to Haidary et al. [4], an experimental investigation was conducted to study the effect

of surface roughness on heat transfer performance in horizontal and vertical heating tubes. The results indicated that rough heating tubes significantly enhanced heat transfer rates compared to smooth tubes. This improvement was attributed to the increased bubble nucleation sites provided by the rough surface, which contributed to better thermal performance under varying experimental conditions. According to Qian et al. [5], research was conducted on droplet velocity in microchannels and its effect on transport time in microscale systems. The study demonstrated that the velocity of droplets in microchannels was significantly higher than the superficial mixture velocity, leading to enhanced heat transfer efficiency. The researchers utilized a novel imaging technique to accurately determine droplet velocity under various conditions, thereby contributing to a deeper understanding of heat transfer dynamics in microchannels. Harirchian and Garimella [6] detected that the reduction of pressure significantly influenced by the channel size and mass flow with FC-77 in microchannels in flow boiling investigations. The heat transfer coefficient was not affected when a specific heat flow and a mass flux were evaluated.

Similar to Al Zaidi et al. [7], the effect of facet proportion ($\beta=W/H$) on the heatwave transference of HFE-7100 in level multiple channels were studied. Constant the hydraulic width, the sordid region, moreover the average superficial roughness, the facet ratios of 0.5, 1, and 2 were considered. The researchers discovered that the facet proportion of the channel had a significant impact on the heat transference in the tested range. The volume of the bubbles in the larger facet proportion

was smaller than the volume of the bubbles in the smaller facet proportion. The length of the slug increased as the aspect ratio decreased. Furthermore, the heat transfer coefficient exhibited a positive correlation with the heat flux, whereas the mass flux had a negligible impact. As aspect ratio increased, local heat transfer coefficient increased. Finally, they recommended studying the flow and thermal characteristics of channels with varied aspect ratios.

These probing of Singh et al. [8] studies the effect of changing the facet ratio of elliptical microchannels on every decrease of aqua vapor stress. Rectangular microchannels with a fixed length of 20 mm and a hydraulic diameter of $142 \pm 2 \mu\text{m}$ were subjected to various aspect ratios (β). The profilometer and pressure drop measurements of hydraulic diameter in single-phase fluid flow exhibit a high degree of consistency. The results indicate that the pressure reduction in rectangular microchannels is at its minimum when the aspect ratio is approximately 1.6 during two-phase flow. The minimal value is likely due to the opposing influences of frictional and accelerating pressure drops with respect to the aspect ratio. Within a specific range of heat flux and mass flow, it was observed that the pressure drop in the two-phase condition was lower than that in the single-phase state. This study was one of the initial inquiries to examine the impact of aspect ratio on the behavior of two-phase flow in microchannels.

An experimental examination was conducted by Soupremanien et al. [9] to study the flow boiling of Forane® 365 HX in two single rectangular horizontal minichannels. The minichannels exhibited different dimensions, although possessed an identical hydraulic diameter of 1.4 mm. The study examines the comparison of two aspect ratios: 0.143, which corresponds to a larger cross-sectional area, and 0.43, which corresponds to a smaller one. The investigations shown that the characteristics of the onset of nucleate boiling (ONB) can be influenced by changes in aspect ratio, namely by reducing the cross-sectional area. Additionally, it was noted that the aspect ratio of 0.143 led to decreased pressure drop values in all the flow boiling experiments.

The investigation by Wang and Sefiane [10] revealed that the aspect ratio had a significant influence on the flow boiling regime, and the heat transfer was significantly influenced by the mass flux in channels with larger hydraulic diameters. Harirchian and Garimella [6] conducted additional research to examine the impact of channel size on heat transmission in microchannel heat sinks using FC-77 and flow boiling. Therefore, the heat transfer coefficient remains consistent in microchannels wider than $400 \mu\text{m}$, as long as the heat flux on the wall remains unchanged.

The aim of this review article by Hussein et al. [11] is to offer a thorough examination of the most recent studies on microchannel heat sinks, specifically emphasizing single-phase flow, flow boiling, and coating microchannels. The purpose of the review is to emphasize the advancements in this particular area and pinpoint the obstacles that must be overcome in order to encourage the widespread use of microchannel heat sinks. The review article critically assesses the scientific investigations conducted on microchannel heat sinks, focusing on the outcomes pertaining to single-phase flow, flow boiling, and the application of coatings on microchannels. The study of single-phase flow in microchannels examines the influence of many factors, such as channel dimensions, fluid characteristics, and flow circumstances, on the rate of heat transfer. The analysis of flow boiling in microchannels involves identifying the

potential benefits and difficulties related with this method.

Wang et al. [12] conducted more research on the effects of tilt on the convective boiling performance of a microchannel heat sink with a diameter of $825 \mu\text{m}$. The study used HFE-7100 as the working fluid. Furthermore, the angle of descent was -90° , whereas the angle of ascent was 90° . Considering the results obtained, it was ascertained that layout decrease results in heat transfer efficiency decrease at the same rate in all cases. For example, if the mass flux is $100 \text{ kg/m}^2 \text{ s}$ and configuration angle 45° , then the heat transfer coefficient is decreased approximately in half. It is equally important to note that as far as buoyancy is concerned the velocity of slug bubbles increases for the upward inclination, and therefore the rise of the heat transfer coefficient.

A novel study conducted by Candan et al. [13] focused on examining the saturation flow boiling characteristics of deionized water in discrete rectangular minichannels. The minichannels had a hydraulic diameter of 1.2 mm and a length of 48 mm. The minichannels have an aspect ratio ($\beta=W/H$) that varies between 0.25 and 4. This experiment examined various combinations of mass flux and wall heat flux levels. Flow visualization is an additional tool that aids in our understanding of flow phenomena at a fundamental physical level. The findings indicate that the channel aspect. The frequency has a significant effect on both the local two-phase heat transference coetaneous moreover the total stress decrease. Based on their findings, the optimal level of performance was achieved when the value of β was set to 1. This occurred due to the presence of a continuous layer of liquid film at the acute angles of the square channels. Conversely, the lowest degree of performance was found when the value of β was set to 0.25. This was due to an early instance of localized dehydration. The study found that the heat transfer coefficient at the channel outlet rises in correlation with the heat flow, mass flux, and vapor quality. The researchers determined that nucleate boiling is the primary mechanism for heat transfer, with bubbly/slug flow being the most prevalent.

Thus, the objective of the current research was to establish the effects of the channel aspect ratio on flow characteristics, pressure gradient, and heat transfer coefficients. They used constant values of the average surface roughness that the average hydraulic diameter was kept constant. The detailed configuration of the test increased the hydraulic diameter of a copper heat sink and we focused on the range of 0.42-2.4 for the channel aspect ratio. The average surface roughness of all channels was determined to be around 18.64 nm. The trials were carried out utilizing deionized water as the fluid, while ensuring that the system pressure remained near 1 bar. We maintained the inlet sub-cooling at a minimal value of 20 K. The mass flux exhibited a range of values between 250 and $450 \text{ kg/m}^2/\text{s}$, while the wall heat flux spanned from 3.1 to 660.3 kW/m^2 .

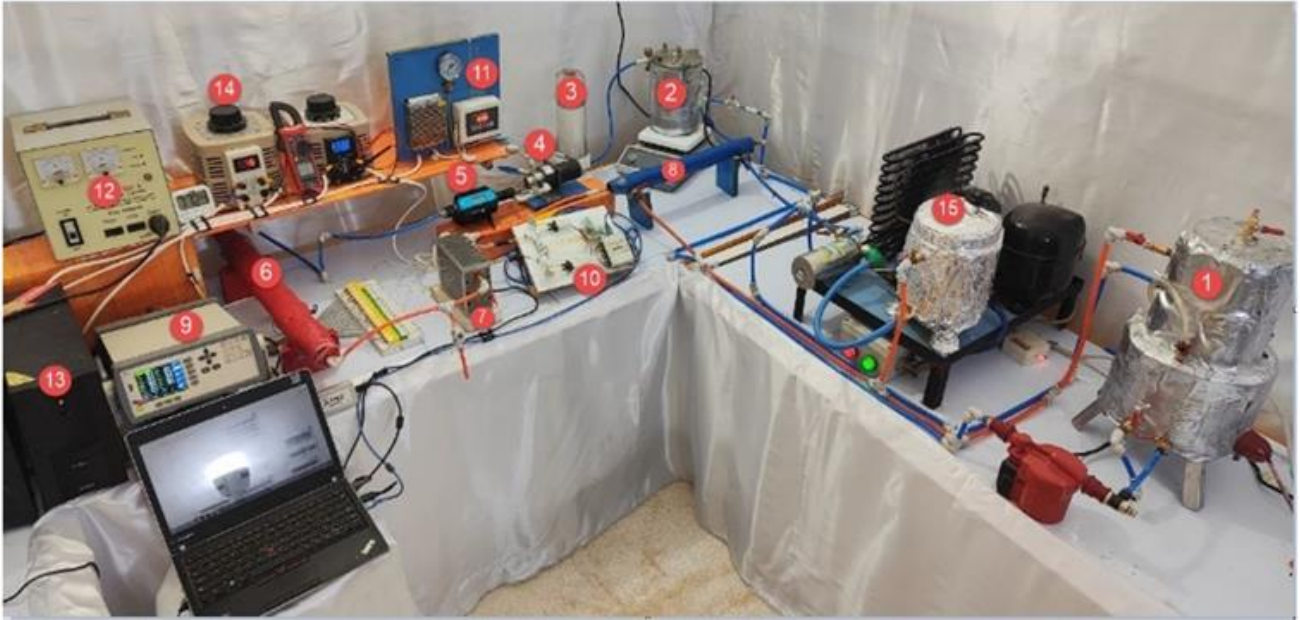
2. INSTRUMENTS AND METHODOLOGY FOR DATA REDUCTION IN EXPERIMENTAL RESEARCH

2.1 Setup experiment

To conduct the experiment, a custom apparatus was built and manufactured. The experimental arrangement consists of a reservoir of deionized water, a miniature gear pump, a device for heating the water before it enters the test area, the actual test area, a device for cooling the water after it leaves the test

area, and a filter placed in the water flow. A rotameter of the LZB-WBF type, with a precision of ± 0.51 ml/min, was employed to measure flow rates across a wide range. Furthermore, a sub-cooler and condensing unit were employed for the purpose of cooling. Figures 1 and 2 depict the schematic design and setup of the experimental system. In order to collect gasses and deionized water in the liquid tank, a process of vigorous boiling was utilized for a duration of one hour. A valve that is open at the topmost part of the condenser

allows the non-condensable gases to be released into the environment. Prior to the installation of the gear pump, a $5\ \mu\text{m}$ filter is employed to eliminate particulate matter from the deionized water. Later, water that was deoxygenated, that is, its dissolved gases were removed, was introduced into the laboratory area. To regulate the temperature of the working fluid, a pre-heater was hired that guaranteed specific control of the input heat.



1- Deasser; 2- Main tank; 3- Filters; 4- Micro-piping pump; 5- Testing area; 6- Pre-heater; 7- Flotation meter; 8- Sub cooler; 9- Data logger; 10- Unit power supply; 11- Pump custodian; 12- AC stability; 13- DAQ- NI- 6009; 14- Variac; 15- Chiller unit

Figure 1. Experimental efficiency

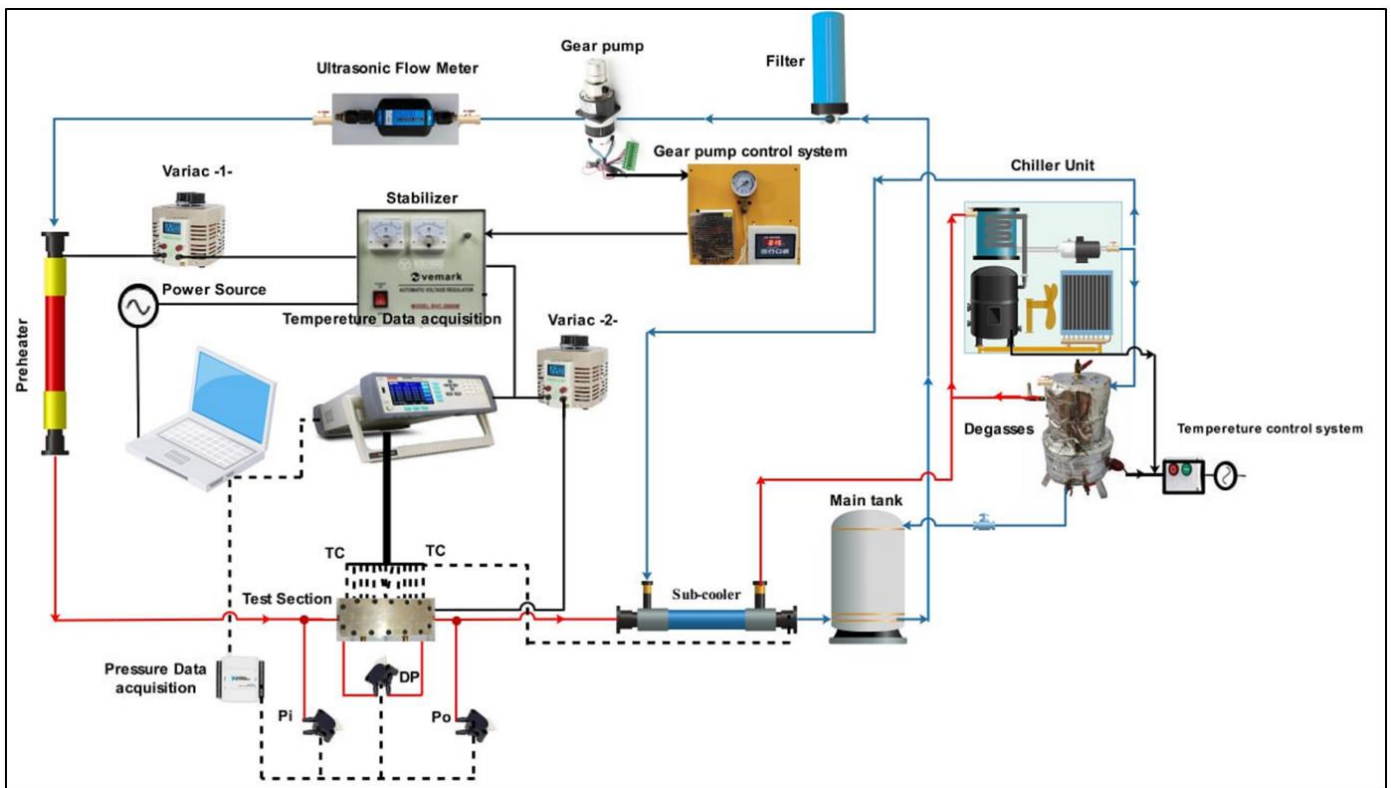


Figure 2. Theoretical explanation of the experimental conventions

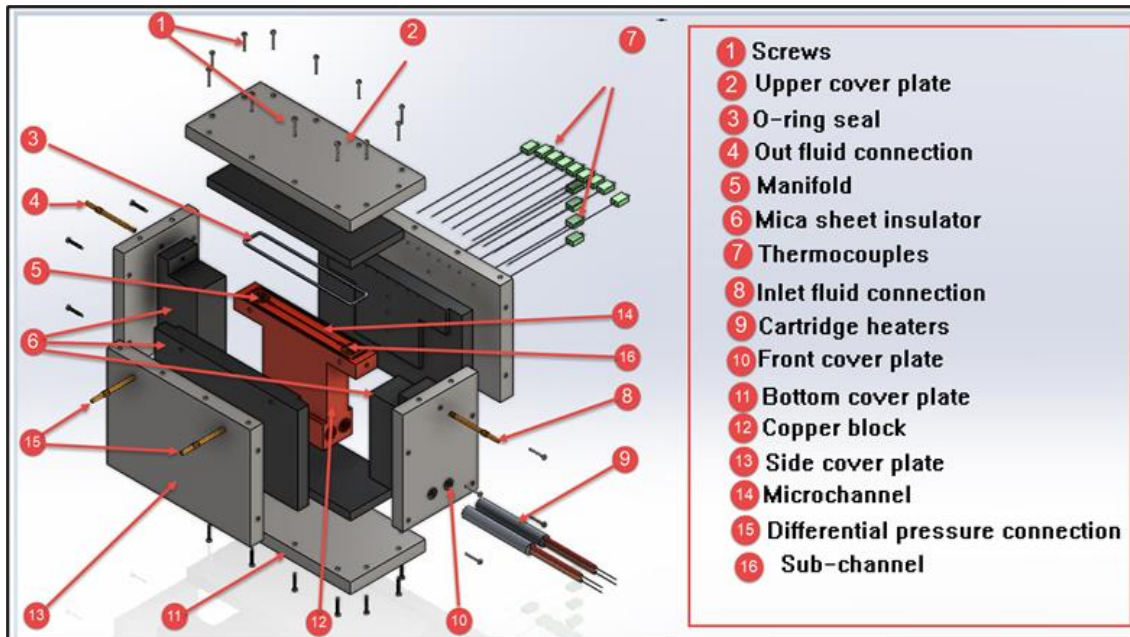
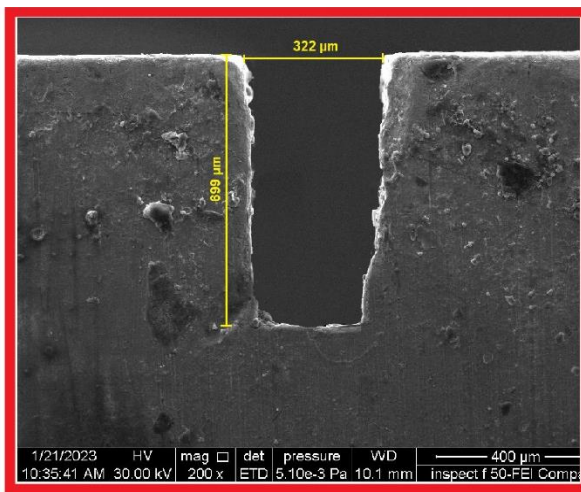
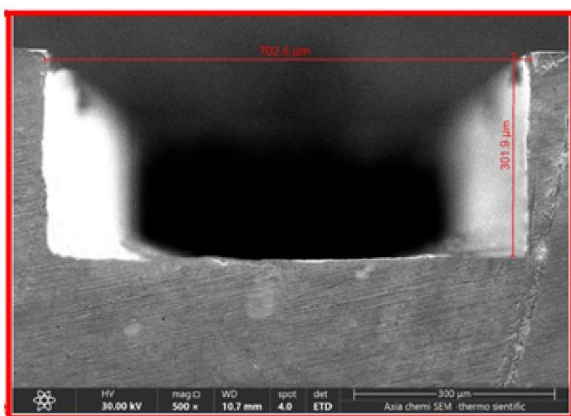


Figure 3. Schematic of the test section



AR=0.42

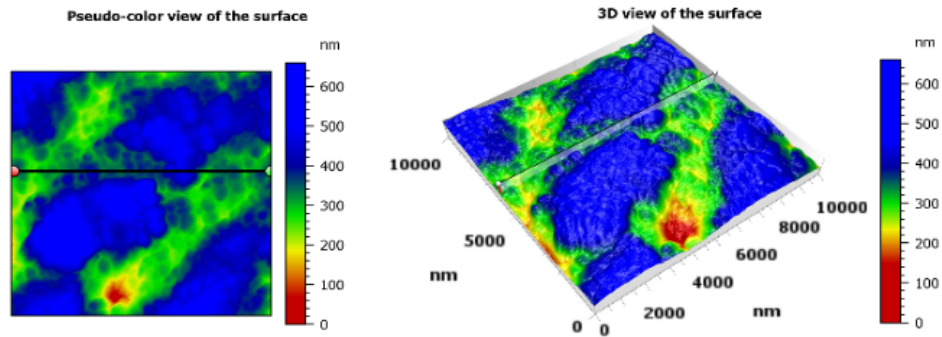


AR=2.4

Figure 4. Micro-channel real dimensions

Copper with one micro-channel, stainless steel casing, top cover plate, and cartridge heaters comprise the experiment

portion. A milling machine feeding at ten millimeters per minute grooved a single rectangular microchannel on the brass block's top surface. The brass object measured 81 mm in height, 30 mm in breadth, and 114 mm in length. The initial microchannel was machined to a depth of 0.7 mm and a width of 0.3 mm; the subsequent microchannel was machined to a depth of 0.3 mm and a width of 0.7 mm. At the base of the brass block were two 100 W cartridge heaters arranged horizontally to provide the required heat. To monitor wall temperature, four type-k thermocouples were evenly placed 14.7 mm vertically along the brass block's center line. Seven microchannel's lower surface depth of 1 mm. All utilized thermocouples had a diameter of 0.5 mm and a calibration error of ± 0.5 k. Figure 3 shows the brass block joined with an angled stainless casing sealed with oaring. The stainless-steel housing is equipped with subchannels as well as inlet and outlet manifolds. Two type-K thermocouples were submerged in subchannels in order to measure the inlet and outlet temperatures of the working fluid. In order to quantify the inlet and exhaust of the pressure out manifold, two MPX5500DP transducers were utilized. However, a differential pressure transducer (MPX4250DP) measured test segment pressure reduction. The transducers had accuracy of ± 3.21 , 4.32, and 4.33%. Manifolds and subchannels were $20 \times 20 \times 0.7$ mm and $7 \times 2 \times 0.7$ mm, respectively. The top covered plate included a visualization window to show flow. The subchannels and window were the same size as the microchannel. The temperature data that was acquired was documented using an Applent AT 4532x data logger. The microchannel's width and depth were determined using an electronic microscope (SEM). The microchannel's dimensions are shown in Figure 4. Microchannel bottom surface irregularity was measured using an atomic force microscope (AFM). Figure 5 illustrates how the average irregularity of the area scanned by the microscope probe, which measured $100,000 \times 100,000$ nm, was 18.64 nm. With the NI USB-6009 Bus-power multifunction DAQUSB model serving as an interface instrument, the LabView software collected the signals (which ranged from 0 to 5 DC-Volts) from the pressure transducer gauge.



ISO 21920 - Roughness (S-L)			
F: [Workflow] Leveled (LS-line)			
S-filter (As): None			
L-filter (Ac): Gaussian, 0.005 mm, Ends not cut			
Evaluation length: All Ac (1)			
Height parameters			
Rq	25.14	nm	Root mean square height
Rsk	0.2482		Skewness
Rku	3.542		Kurtosis
Rt	123.7	nm	Total height
Rp	64.57	nm	Maximum hill height
Rq	64.57	nm	Mean hill height
Rv	59.14	nm	Maximum dale depth
Rv	59.14	nm	Mean dale depth
Rz	123.7	nm	Maximum height
Rz	123.7	nm	Mean height
Ra	18.64	nm	Arithmetic mean absolute height
Spatial parameters			
Ral	429.2	nm	Autocorrelation length
Rsw	3324	nm	Dominant spatial wavelength
s	0.2		
Hybrid parameters			
Rdq	9.873	°	Root mean square gradient
Rda	7.764	°	Arithmetic mean absolute gradient
Rdt	30.66	°	Maximum absolute gradient
Rdl	5089	nm	Developed length
Rdr	1.482	%	Developed length ratio
Material ratio parameters			
Rmr	100.0	%	Material ratio
Rmc	49.52	nm	Inverse material ratio
Rdc	31.90	nm	Profile section height difference
c	1000	nm	below highest peak
p	20%		
q	80%		
Feature parameters (element)			
Rsm	1582	nm	Mean width of the profile elements
Rsmx	2861	nm	Maximum profile element width
Rsmq	1344	nm	Standard deviation of profile element widths
Rc	74.41	nm	Mean height of profile elements
Rcx	107.3	nm	Maximum height of profile elements

Figure 5. The probing of the topography of the superficial in every micro-channel's undermost expanse (10000 nm × 10000 nm)

2.2 Adjustment procedure

2.2.1 Thermocouple adjustment

An accurate mercury thermometer calibrated the thermocouples. A mercury thermometer was placed next to each thermocouple in a distilled water conduit. The thermocouple and thermometer values were recorded from 0°C to 99°C, rising by about 10°C every interval. The thermocouple accuracy was found to be between ±0.2 and ±0.7.

2.2.2 Pressure transducer calibration

We used a deadweight tester to calibrate the pressure transducer. The tested pressure transducer was subjected to pressures generated by calibrated weights in this tester. The result is a certain voltage at the output. In order to document its findings, it was connected to a data collection device. Consequently, the LabVIEW software was used to record the values of the output voltage. It was found that the transducers for input pressure, output pressure, and differential pressure were accurate to within ± 4.32%, ± 3.21%, and ± 4.33 mm,

respectively.

2.2.3 Rotameter calibration

The static calibration approach was used to calibrate three rotameters. This method measures the flow rate of de-ionized water, which is heated to 25°C, by passing it through a rotameter. A borosilicate glass burette was used to measure the quantity over time; its capacity range was 0-25 ml. We compared the rotameter readings to the volume measured within the allotted time frame. The high-range, medium-range, and low-range rotameters were calibrated with accuracies of ±0.51, ±0.407, and ±0.358 ml/min.

2.3 Data reduction

A net pressure drops, indicated by ΔP_{ch} , occurs in single-phase flow through a microchannel and may be expressed as [14]:

$$\Delta P_{ch} = \Delta P_{lm} - \Delta P_{loss} \quad (1)$$

ΔP_{lm} is the quantitative representation of the pressure differential between the input and output manifolds. A number of minor losses, such as the input sub channel $\Delta P_{sch,i}$, the output sub channel $\Delta P_{sch,o}$, the abrupt contraction ΔP_{sc} , and the abrupt expansion ΔP_{se} , contribute to the pressure drop represented by ΔP_{loss} . Thus, it might be calculated as [14]:

$$\Delta P_{loss} = \Delta P_{sch,i} + \Delta P_{sch,o} + \Delta P_{se} \quad (2)$$

Due to the quick contraction and expansion, the pressure reduction brought on by all of the microscopic losses was computed using Eq. (3) [14]:

$$\Delta P_{loss} = \frac{(K_{sc1} + K_{se2}) \cdot (V_{sch}^2 \cdot \rho)}{2} + \frac{(K_{sc2} + K_{se1}) \cdot (V_{ch}^2 \cdot \rho)}{2} \quad (3)$$

Moving from a multichannel to a subchannel, and then from a subchannel to a minichannel, decreases the volume extremely. This alteration in volume is expressed through the loss parameters, K_{sc1} and K_{sc2} . Other than the coefficient K_{se1} and K_{se2} , which represent the pressure loss/gain from the transition from the microchannel to the subchannel, and then to the manifold.

The values for the loss coefficient are calculated as follows: $K_{sc1} = 0.5$, $K_{sc2} = 0.47$, $K_{se1} = 0.72$ and $K_{se2} = 0.81$.

Based on the aforementioned values, the coefficient of friction for the experiments can be estimated using the following formula, which is derived from the pressure drop in the microchannels [14]:

$$f_{ch} = \frac{\Delta P_{ch} \cdot D_h}{2\rho L V_{ch}} \quad (4)$$

At the heat sink, the base heat flow (\dot{q}_b) was calculated using Eqs. (5) and (6) [15]:

$$\dot{q}_b = \frac{P - Q_{loss}}{A_b} \quad (5)$$

$$P = I \cdot V \quad (6)$$

The thermal power in watts is expressed by (P), and the electrical current in amperes is expressed by (I). For the electrical voltage, it is expressed in volts by the term (V), the base area of the heatsink is indicated (A_b).

The base area is derived by taking the core heating width of the base plate, W_b , and the core heating length of the base plate, L_{ch} , and integrating them to calculate the base area.

$$A_b = W \cdot L_{ch} \quad (7)$$

Calculating the heat loss (Q_{loss}) from a test area to its surroundings may be achieved by heating it without pumping liquid. Measured and recorded are the power and temperature of the bottom wall of the microchannel after the system has reached a steady condition.

The other electrical power levels are obtained by performing the preceding operations successively. In several works, authors have drawn the heat loss equation on the XY graph depicting the electrical power supplied, against the temperature difference of the bottom wall and the surrounding temperature. Researchers have begun and will continue to employ this approach [14, 15].

The coefficients of local heat transport $h_{sp}(z)$ are determined [16] as shown in follows:

$$h_{sp}(z) = \frac{\dot{q}_b \cdot W}{(T_w(z) - T_f(z)) (W_{ch} + 2H_{ch})} \quad (8)$$

The height of the channel is denoted by H_{ch} , and its width by W_{ch} . It was chosen to place thermocouples close to the microchannel base, one millimetre away. In order to ascertain the internal surface temperatures $T_w(z)$ of the microchannel, the temperature data from the thermocouples $T_{tc}(z)$ were calculated again employing a one-dimensional heat conduction formulation, as demonstrated in Eq. (7) [13]:

$$T_w(z) = \frac{T_{tc}(z) - (\dot{q}_b th)}{K} \quad (9)$$

Table 1. Value of uncertainty for every measured parameter

Variable Quantity	Measurement Tool	Uncertainty Value	Sources
The fullness of microchannel	Inspect 50 FE -SEM	± 0.011 mm	The company's inspection system F50 FE-Sem is effective.
The length of microchannel	Inspect 50 FE -SEM	± 0.022 mm	The company's inspection system F50 FE-Sem is effective.
The length of microchannel	Vernier caliper	± 0.04 mm	Manufacturing
voltage and current alternation	Voltmeter	± 0.4 V	Model (DT200)
Alternating current	Clamp meter	± 0.02 A	Model of the clamp meter (UNI-TUT202+)
The total volume of the flow	Low rotameter range	± 0.245 ml/min	Calibrated
	Medium rotameter range	± 0.311 ml/min	Calibrated
	High rotameter range	$\pm (\pm 0.32)$ ml/min	Calibrated
Pressure	Differential pressure transducers-model MPX4250	± 0.0211 bar	Calibrated
	Different pressure differential converters-model MPX5500	± 0.0144 bar	
Temperature	The data logger and the thermocouple that is RS-Pro-K	$\pm (0.1-0.5)^\circ\text{C}$	Calibrated

Assuming a uniform boundary condition, the localized fluid temperature $T_f(z)$ can be calculated using Eq. (9) [14]:

$$T_f(z) = T_i + \frac{\dot{q}_b \cdot W \cdot z}{m C_p} \quad (10)$$

where, T_i denotes the intake fluid temperature, and C_p represents its temperature. The axial length of the channel, the bulk flow rate, and the particular heat of the fluid are all measured.

To determine the average Nusselt number, Eq. (11) was applied [17]:

$$Nu = \frac{1}{L_{ch}} \int_0^{L_{ch}} \frac{h_s p(z) \cdot D_h}{K_l} dz \quad (11)$$

Bernoulli's apparatus has significantly advanced the experimental understanding of Reynolds numbers and their applications in analyzing thermal and fluid systems [18].

The experiments were conducted using deionized water as the working fluid and a system pressure of 1 atm, a heat flux of 60.225 kW/m², and a Reynolds number range of 283-4840.

The discrepancy between the measured quantity's real value and its measurement-acquired value is known as measurement error. It may arise from several factors and encompasses both random and biased errors. The measuring equipment's inaccuracy causes bias error, which may be decreased via device calibration. Outside factors like ambient temperature, pressure, humidity, etc., cause accuracy errors, also known as random errors. Table 1 summarizes uncertainty in all measured quantities [19].

3. RESULT AND DISCUSSION

3.1 Friction factor

A plot with the comparison with the experimental result as given in the literature and the interaction between the developing flow and the fully developed flow in a laminar flow option as per Shah and London [20]. It was also followed in the usage of the apparent friction factor f_{app} of the developing flow in the laminar zone starting the year 1978 from the correlation developed by Shah and London [20]:

$$f_{app} = \frac{3.44}{Re(L^*)^2} + \frac{f_{FD} Re + \frac{K(\infty)}{4L^*} - \frac{3.44}{(L^*)^2}}{Re(1 + C(L^*)^{-0.2})} \quad (12)$$

$$L^* = \frac{L_{sp}}{Re D_h} \quad (13)$$

Both $(K(\infty))$ and (C) are constant, although their values rely on the aspect ratio of the present research, which is (1.7784×10^{-4}) and (1.1962) . Similarly, Shah and London [20] expressed the Poiseuille number $(f_{FD} Re)$ of fully developed single-phase fluid flow.

$$f_{FD} Re = 24(1 - 1.35534\beta + 1.9467\beta^2 - 1.7012\beta^3 + 0.9653\beta^4 - 0.2537\beta^5) \quad (14)$$

$$\beta = \frac{W_{ch}}{H_{ch}} \quad (15)$$

Furthermore, the study examined the links between flow development in turbulent flow zones and the distinction between developing and developed flow in Phillis and Blasius. The Blasius Correlation of Fanning friction factor may be used to fully form turbulent flow [21].

$$f = 0.079 Re^{-0.25} \quad (16)$$

Additionally, it is found that the fanning friction factor for turbulent flow generation [21]:

$$f_{appturb} = \frac{0.0929 + 1.0161 D_h}{L} Re^* \left(-\left(\frac{0.268 + 0.3193 D_h}{L} \right) \right) \quad (17)$$

where, Re^* represents the equivalent Reynolds number, which can be calculated as follows:

$$Re^* = Re \left(\frac{2}{3} + \frac{11}{24} \beta (2 - \beta) \right) \quad (18)$$

Figure 6 shows how the fanning friction factor and Reynolds number relate in conventional microchannels. Comparing these findings with those of different studies, it is evident that Shah and London [20] proposed a correlation for laminar flow, with a mean absolute error (MAE) of 1.58%. Additionally, a comparison was made with Mohamed's results, where the difference was found to be 1% [22].

The experimentally determined Fanning friction factor is about the conventional and coated microchannel's Reynolds number, as seen in Figure 6. Shah and London [20] identified a link for laminar developed flow and forecasted with a 1.58% MAE.

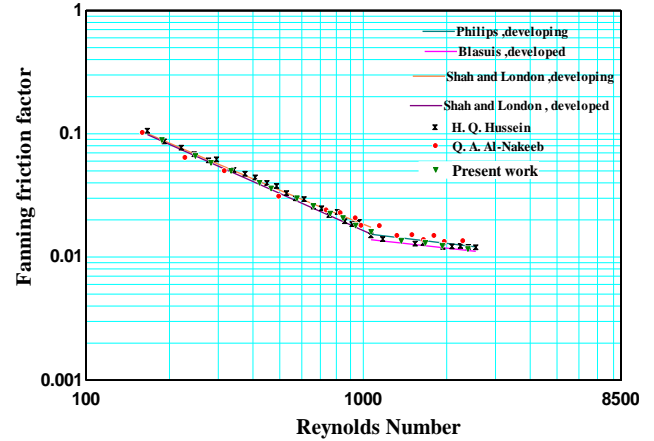


Figure 6. Experimental Fanning friction factor results compared with laminar and turbulent flow correlations and experimental for microchannel

$$AE = \frac{1}{N} \sum_{j=1}^N \frac{|f_{(pred,j)} - f_{(exp,j)}|}{f_{(exp,j)}} \times 100\% \quad (19)$$

Shah and London [20] correlation for laminar developing flow also compared fairly well with the present results mean absolute error (MAE) of 1.89%. In addition, it was ascertained that the association was supported by the data. On the other hand, concerning two models located within a turbulent region at full maturity, the experimental outcomes have been also estimated using Blasius's correlations established in 1913 with the overall MAE of 2.57%.

The mundane distance between the occurrences of turbulent

flow development was efficaciously determined, the average entire error (MAE) was approximately 2%. However, as is depicted in Figure 6, a comparison between the laboratory results of study [15] and the current study have a MAE of 8.07%. This insinuate that the likely values in this study are greater than the noted MAE of 2.9% by Hussein [23] in his study on the accouterments of sub-optimal conditions on enzyme performance.

Overall, the text defines how to utilize customary methods to understand the causes of friction in single-phase flow in microchannels and in laboratory circumstances. Customary flow theory states that as the Reynolds number augmentation, the consequence of fresh flow theory increases, this additionally leads to a higher traction factor for all models in the laminar locale. In this regard, the equalization was reference, this equalization uses a numerary value of 20 to calculate the length of the hydrodynamic flux in the laminar territory [24]:

$$L_{hy} = 0.056 Re D_h \quad (20)$$

Since all microchannel models have the same hydraulic diameter, if the Reynolds number is constant, their hydrodynamically evolving lengths will be the same.

3.2 Heat transfer

The spider web-like MEMS accelerometer design demonstrates exceptional sensitivity and robustness, making it a viable solution for high-precision sensing applications [25].

The typical average Nusselt number and Reynolds number in laminar flow conditions is related to a range of numbers (166-2500), as shown in Figure 7. The results demonstrate that the average Nusselt number of customary and jacket microchannels increases with every Reynolds number. This pattern demonstrates the ongoing evolvement of heat transfer theory. The lack of the relaxation phase in this investigation may be the primary cause of this trend. As a result, the flow is increased by the thermic expansion. "Enhanced heat transference" is the presence of a thin thermic boundary layer in areas that still have heat to be transferred, this enhances the heat transfer rate similar to areas that have already generated all their heat. The magnitude of the thermal expansion length can be accomplished using the equation advanced by Shah and London in 1978 [20].

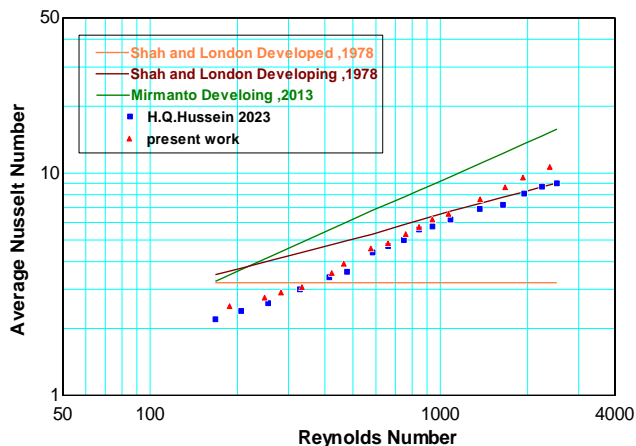


Figure 7. Experimental average Nusselt number results compared with laminar flow correlations and experimental microchannel

$$L_{th} = 0.056 Re Pr D_h \quad (21)$$

From Eq. (21) it is observed that the thermal entry length increases with the Reynolds number and it can occupy the entire channel length at $Re \approx 510$. The relationships also indicate those postulated by Shah and London [20] and Al-Nakeeb et al. [21], and the predicted average value for Nusselt number in microchannels containing conventional and coated sections and the experimental values for the laminar area in parallel to each other.

$$Nu = 8.235(1 - 10.6044\beta + 61.1755\beta^2 - 155.1803\beta^3 + 176.9203\beta^4 - 72.9236\beta^5) \quad (22)$$

$$Nu = 0.775 L_t^{*\left(-\frac{1}{3}\right)} (f Re)_{FD}^{\left(\frac{1}{3}\right)} \quad (23)$$

where, L^* denotes the dimensionless length of the channel and can be mathematically represented as follows [23]:

$$L_t^* = Re^{0.283} Pr^{-0.513} L_t^{*(-0.309)} \quad (24)$$

Comparison of the current study's results with the predicted values derived from Shah and London correlations [24] for fully developed flow showed poor prediction criteria, where MAE was 26.13%. On the other hand, comparing the results of the microchannel with the Shah and London correlation for developing flow twelve percent of the samples were outside the trend line for estimating the ordinary microchannel with an MAE of 15.12%. In the meanwhile, the comparison with the correlation of Mirmanto [24] for the microchannel yielded poor prediction of the plain microchannel results with the MAE of 25.63% for 59.47%. This could be because the correlation that had to be made had to take into account the significant impact.

However, it is seen from the figure that the comparison results of the present work with the earlier experimental data [24] were reasonable with the MAE of 4.46%. To summarize, according to the outcomes of the single-phase flow experiments, the measurement and calibration system is sufficient in performing two-phase flow investigations. Boiling curve with heat flux raise for $Z/L = 0.98$ in the micro channels for mass flux varying from 250 up to 450 with step 100 and $\Delta T_{sub} = 20$ K is shown in Figure 8. The values of the wall heat fluxes range from 0 to 625.1 kW/m². It is indicated in Figure 8 that the boiling curve of the surface shifts towards the left-hand side as the mass flux is increased (delay of onset nucleation boiling with increasing mass flux).

But when the boiling curves of the different aspect ratios as shown by Figure 8 (a, b and c), it was observed that the wall superheat needed to trigger boiling in the high aspect ratio channel was lower as compared to low aspect ratio channel. For example, at the mass fluxes of 250 and 450 kg/m²s, the wall superheat on the outside of the channels with high aspect ratios was equal to 2.2 and 4.1 K correspondingly.

On the same note, wall superheat on these channels with small aspect ratios was estimated to be about 2.7 and 4.4 K correspondingly. Surfaces with a higher aspect ratio may cause a significant increase in the active nucleation sites on the heated surface that is, the number of cavities that form on the surface. This in return results in a decrease in the level of wall superheat on the side of the channel that possesses the higher aspect ratio for the specified wall heat flux.

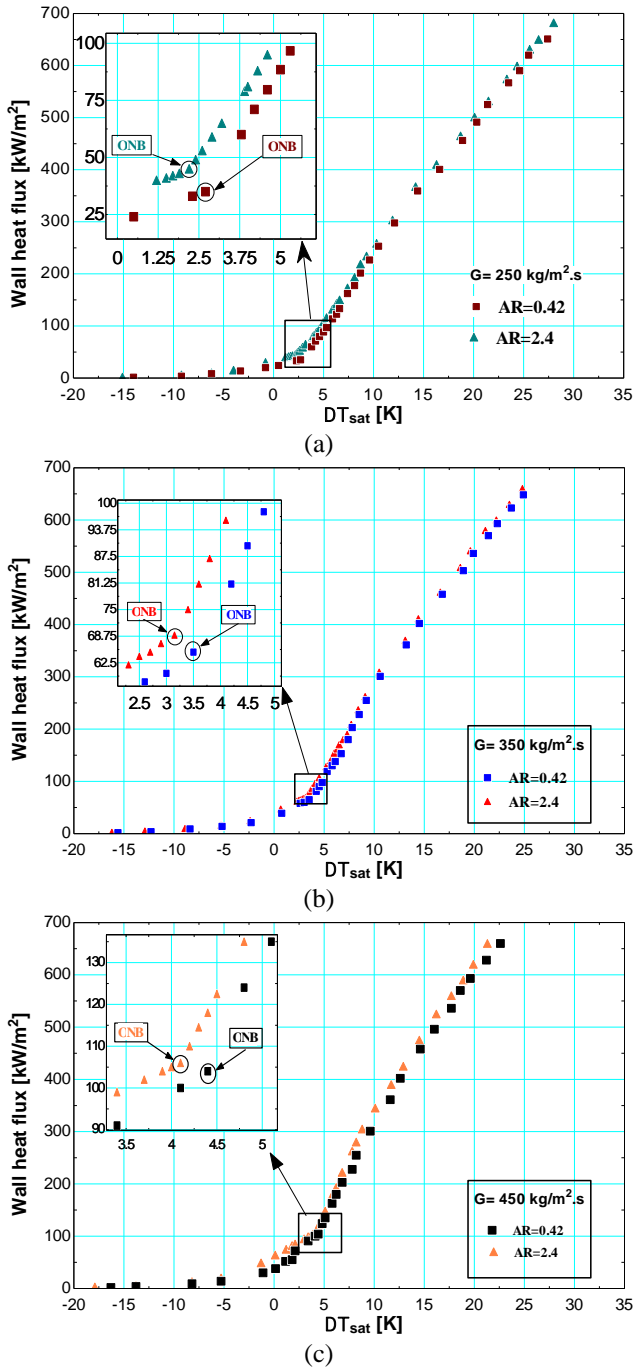


Figure 8. Boiling curve for different aspect ratio of microchannel over range of mass fluxes at degree sub-cooled 20 K and location ($Z/L_{ch} = 0.98$)

However, comparison has been made in respect of the distinct proportion of facet for the microchannel in terms of every local temperature difference and as illustrated in Figure 9(a-c), at low and high mass flux. Raising the heat transfer coefficient is rather slower at the mass flow rate of $250 \text{ kg/m}^2 \cdot \text{s}$ than at the mass flow rate of $450 \text{ kg/m}^2 \cdot \text{s}$, especially at high values of q'' , for example, when the mass flux is 250 and 450 $\text{kg/m}^2 \cdot \text{s}$, the maximum increase in HTC based on average on the surface of the Higer to lower aspect ratio channels is equal 6.13% and 4.08%, accordingly. It can be explained, as indicated that the heat transfer coefficient depends to a serious extent on the wettability of the surface and to a lesser extent on the morphology of surface, the increase of the heat transfer coefficient for the higher aspect ratio tube may be benefited from the porous structure.

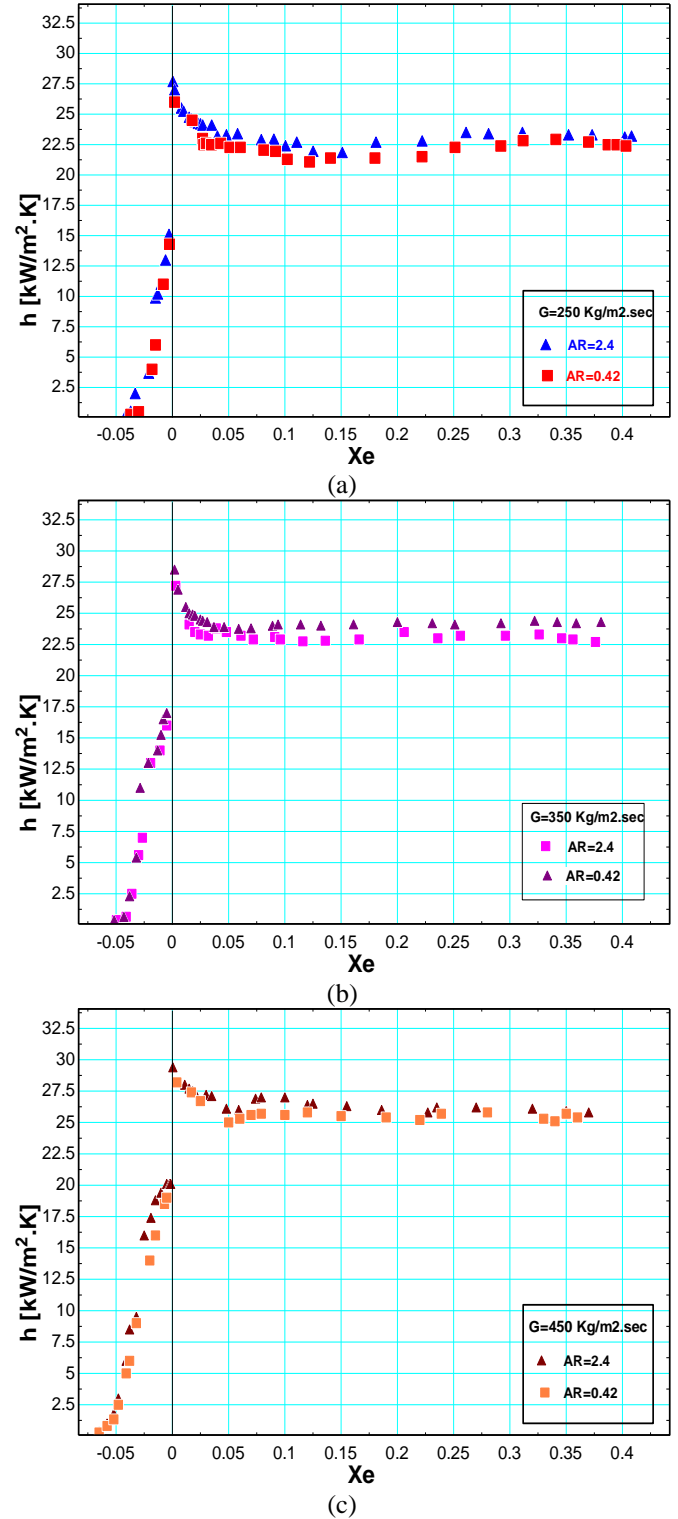
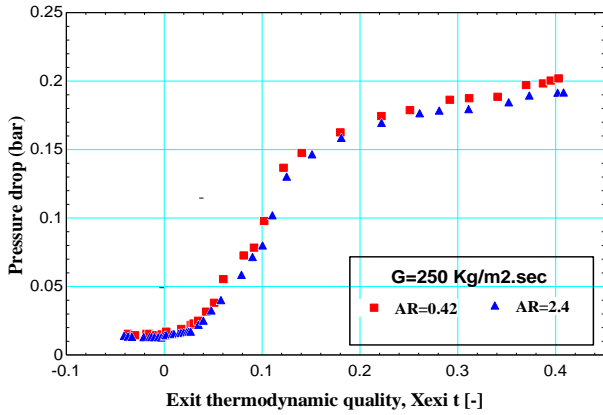
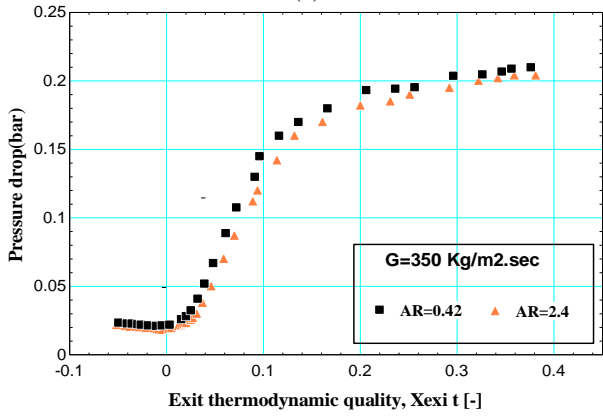


Figure 9. Local heat transfer coefficient versus wall heat flux over range of mass fluxes for different aspect ratio microchannel at location ($Z/L_{ch} = 0.98$) for degree of sub-cooled 20 K

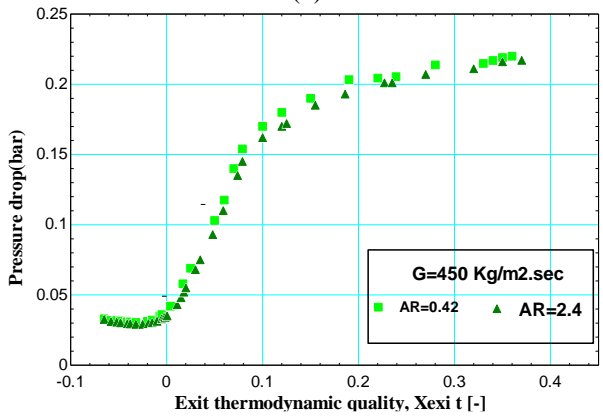
Variation of pressure drop with wall heat flux for the microchannels having different aspect ratio designs for the several mass flux ($250, 350$ and $450 \text{ kg/m}^2 \cdot \text{s}$) can be presented in Figure 10(a-c) at a sub cooling of 20 K. As it can be observed from Figure 10, pressure drop of the boiling flow for the continuous wall heat flux reduces with the increase in the mass flux. This is because the acceleration in the flow as well as the frictional pressure drop in the micro channels rise with the increasing mass flux.



(a)



(b)

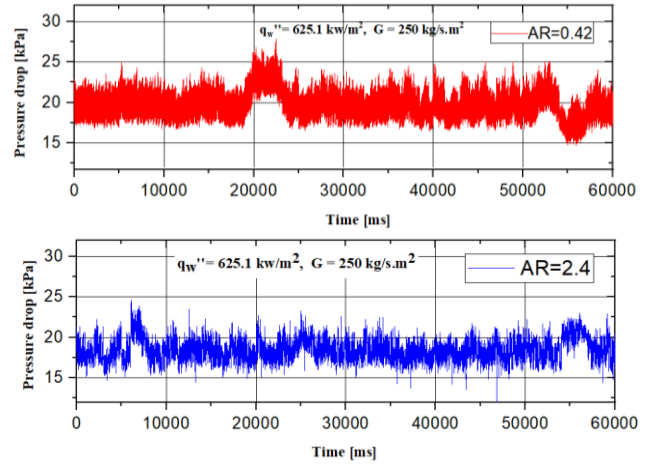


(c)

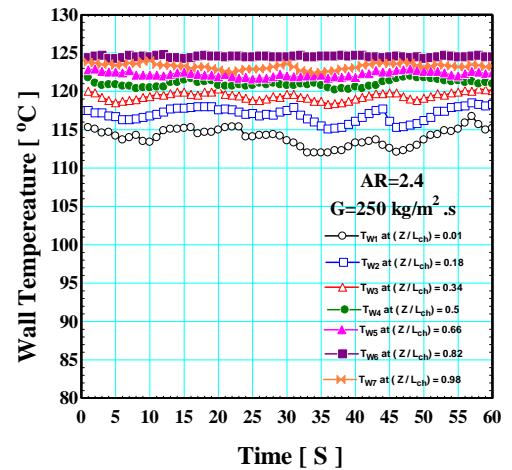
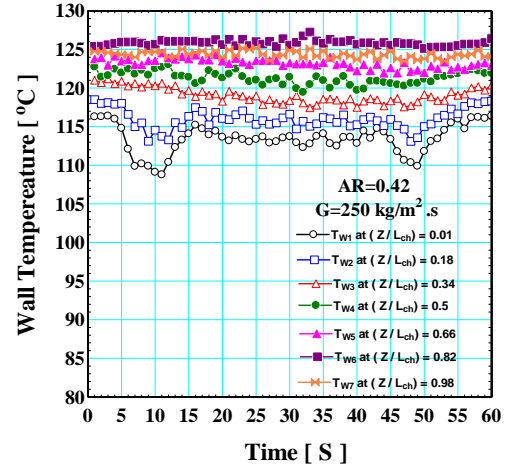
Figure 10. Pressure drops versus the exit vapor quality over range of mass fluxes for different aspect ratio microchannel at degree sub-cooled 20 K

3.3 Flow boiling instability

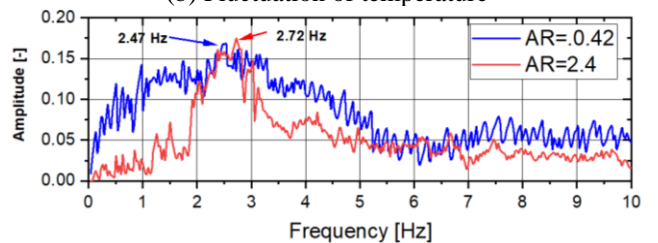
The variation of mass flow rate on the variation in wall temperature of the microchannel, inlet and outlet fluid temperature, and the pressure drop measured is shown in Figure 11(a). In Figure 11, the trace of the fluctuations of the mass flux of the period 60s has been shown where the wall heat flux is kept constant at 625.1 kW/m^2 and degree sub-cooled at 20 K where the mass flux is being increased from 0.42 to $2.4 \text{ kg/m}^2\text{s}$ the oscillations of the trace of outlet water temperature can be observed which indicates that there is a significant scale oscillation. The latter scale oscillations are much more curious at aspect ratio increasing from 0.42 to 2.4, at the duration of 60 seconds, which has a minimal temperature oscillation amplitude of 0.855°C . In comparing it to inlet water temperature the following was noted, the oscillation of water temperature is 2.1°C at 0.42 and 1.89°C at 2.4.



(a) Fluctuation of pressure drop



(b) Fluctuation of temperature



(c) Pressure drop frequency analysis plain microchannel at two mass flux, high wall heat flux

Figure 11. Pressure drop and temperature fluctuations, and frequency analysis in plain microchannels at different aspect ratios ($AR = 0.42$ and 2.4) with two mass fluxes

Further, from the Figure 11(b), for 0.42, very tiny scale oscillations of the axial wall temperatures T_{w1} at the same

period were observed as compared to 2.4. For instance, the oscillation amplitudes in the axial wall temperatures were determined to be $T_{w1} = 2.9^\circ\text{C}$ and when the 2.4, $T_{w1} = 2.68^\circ\text{C}$.

Thus, as pointed out in the previous sections, the actual inception of nucleate boiling was postponed as the aspect ratio increased. Thus, the trends of the amplitude oscillations of the pressure drop were opposite to the changes in the mass flux magnitude. For instance, the pressure drops oscillations of the microchannel with aspect ratio of 0.42 and 2.4 are 2.5 kPa, for the case shown in Figure 11(c). However, based on the presented results, it can be concluded that, in case of increasing the aspect ratio, flow boiling instability is less pronounced at the constant heat flux density. In addition, pressure drop data results were processed using Fast Fourier Transform to establish the frequency distribution for pressure drop for two different aspect ratios constant, heat flux as shown in Figure 11(c). The results shown in this paper unveil how oscillation frequency and amplitude go up in tune to the aspect ratio, taking for example the aspect ratio of 0.42 for which the oscillation frequency and the amplitude are equal to 2.5 Hz and 0.167, respectively, and the aspect ratio of 2.4 for which the oscillation frequency and the amplitude are equal to 2.7 Hz and 0.158.

4. CONCLUSIONS

Experiments involving the heating of deionized water in single-microchannel heat sinks were conducted. Two distinct channel aspect ratios 2.4 and 0.42, were evaluated at a hydraulic diameter of 0.42 mm. The mass flow range for the trials was 250-450 kg/m²s, the wall heat flux range was 0-625.1 kW/m², the system pressure was 1 bar (measured at the test section intake), and the inlet sub-cooling was close to 20 K. The following is a summary of the main conclusions:

- 1). Enhancement of average Nusselt number increasing with increase aspect ratio from 0.42 to 2.4.
- 2). The percentage reduction in wall superheat for increasing aspect ratio from 0.42 to 2.4, 22.7% at high mass flux.
- 3). With maximum increases of 6.13% and 4.08%, respectively, the heat transfer coefficient enhancement under mass flow rates of 250 kg/m²s is less substantial than under 450 kg/m²s, particularly in high heat flux levels.
- 4). The study's findings indicate that the pressure drop decreases as the aspect ratio increases and rises with the wall heat flux.
- 5). As the aspect ratio increased, the initiation of nucleate boiling was postponed. Consequently, the magnitude of the pressure drop's oscillations decreased as the mass flux grew. The pressure drop oscillations for aspect ratios of 0.42 and 2.4 are 2.5 and 2.6 kPa, respectively.

ACKNOWLEDGMENT

The Technology University College of Engineering and Department of Mechanical Engineering supported the current investigation.

REFERENCES

[1] Mudawar, I. (2013). Recent advances in high-flux, two-

phase thermal management. *Journal of Thermal Science and Engineering Applications*, 5(2): 021012. <https://doi.org/10.1115/1.4023599>

[2] Karayiannis, T., Mahmoud, M.M. (2018). Flow boiling in micro-passages: Developments in fundamental aspects and applications. In *Proceedings of the 16th International Heat Transfer Conference (IHTC-16)*, Beijing, China. <http://bura.brunel.ac.uk/handle/2438/16332>.

[3] Diaz, M.C., Schmidt, J. (2007). Experimental investigation of transient boiling heat transfer in microchannels. *International Journal of Heat and Fluid Flow*, 28(1): 95-102. <https://doi.org/10.1016/j.ijheatfluidflow.2006.05.008>

[4] Haidary, F.M., Hasan, M.R., Adib, M., Labib, S.H., Hossain, M.J., Ghosh, A.K., Goswami, A. (2021). Enhancement of pool boiling heat transfer over plain and rough cylindrical tubes. *International Journal of Heat and Technology*, 39(2): 329-336. <https://doi.org/10.18280/ijht.390201>

[5] Qian, J.Y., Li, X. J., Wu, Z., Cao, Z., Sunden, B. (2022). Determination of droplet velocity in square microchannel. *International Journal of Computational Methods and Experimental Measurements*, 10(1): 62-73. <https://doi.org/10.2495/CMEM-V10-N1-62-73>

[6] Harirchian, T., Garimella, S.V. (2008). Microchannel size effects on local flow boiling heat transfer to a dielectric fluid. *International Journal of Heat and Mass Transfer*, 51(15-16): 3724-3735. <https://doi.org/10.1016/j.ijheatmasstransfer.2008.03.013>

[7] Al Zaidi, A., Mahmoud, M.M., Karayiannis, T.G. (2018). Flow boiling of HFE-7100 in multi-microchannels: Aspect ratio effect. In *6th Micro and Nano Flows Conference*, Atlanta, USA. <http://bura.brunel.ac.uk/handle/2438/16045>.

[8] Singh, S., Kulkarni, A., Duttgupta, S., Puranik, B., Agrawal, A. (2008). Impact of aspect ratio on flow boiling of water in rectangular microchannels. *Experimental Thermal and Fluid Science*, 33(1): 153-160. <https://doi.org/10.1016/j.expthermflusci.2008.07.014>

[9] Soupremanien, U., Le Person, S., Favre-Marinet, M., Bultel, Y. (2011). Influence of the aspect ratio on boiling flows in rectangular mini-channels. *Experimental Thermal and Fluid Science*, 35(5): 797-809. <https://doi.org/10.1016/j.expthermflusci.2010.06.014>

[10] Wang, Y., Sefiane, K. (2012). Effects of heat flux, vapour quality, channel hydraulic diameter on flow boiling heat transfer in variable aspect ratio micro-channels using transparent heating. *International Journal of Heat and Mass Transfer*, 55(9-10): 2235-2243. <https://doi.org/10.1016/j.ijheatmasstransfer.2012.01.044>

[11] Hussein, H.Q., Fayyadh, E.M., Hasan, M.R. (2024). A review of single flow, flow boiling, and coating microchannel studies. *Open Engineering*, 14(1): 20220522. <https://doi.org/10.1515/eng-2022-0522>

[12] Wang, C.C., Chang, W.J., Dai, C.H., Lin, Y.T., Yang, K.S. (2012). Effect of inclination on the convective boiling performance of a microchannel heat sink using HFE-7100. *Experimental Thermal and Fluid Science*, 36: 143-148. <https://doi.org/10.1016/j.expthermflusci.2011.09.006>

[13] Candan, A., Markal, B., Aydin, O., Avci, M. (2018). Saturated flow boiling characteristics in single rectangular minichannels: Effect of aspect ratio. *Experimental Heat Transfer*, 31(6): 531-551.

- <https://doi.org/10.1080/08916152.2018.1463305>
- [14] Özdemir, M.R., Mahmoud, M.M., Karayiannis, T.G. (2021). Flow boiling of water in a rectangular metallic microchannel. *Heat Transfer Engineering*, 42(6): 492-516. <https://doi.org/10.1080/01457632.2019.1707390>
- [15] Al-Nakeeb, Q.A., Fayyadh, E.M., Hasan, M.R. (2022). Experimental investigation of artificial cavities effect of single-phase fluid flow and heat transfer in single microchannel. *Engineering and Technology Journal*, 40(1): 109-119. <https://doi.org/10.30684/etj.v40i1.2122>
- [16] Al-Nakeeb, Q.A., Fayyadh, E.M., Hasan, M.R. (2022). Experimental investigation on sub-cooled degree effect on the flow boiling in a microchannel heat sink. In *Proceedings of the 7th International Conference on Production, Energy and Reliability (ICPER 2020)*, Kuching, Malaysia. https://doi.org/10.1007/978-981-19-1939-8_26
- [17] Fayyadh, E.M., Mahmoud, M.M., Sefiane, K., Karayiannis, T.G. (2017). Flow boiling heat transfer of R134a in multi microchannels. *International Journal of Heat and Mass Transfer*, 110: 422-436. <https://doi.org/10.1016/j.ijheatmasstransfer.2017.03.057>
- [18] Mohammed, S.A., Fayyadh, E.M. (2019). Experimental investigation of sub-cooled flow boiling in metallic microchannel. *Engineering and Technology Journal*, 37(10): 408-415. <https://doi.org/10.30684/etj.37.10A.5>
- [19] Adaramola, B.A., Kayode, J.F., Afolalu, S.A., Rominiyi, O.L., Okokpujie, I.P., Ikumapayi, O.M. (2023). Investigating fluid flow regimes: A novel design and implementation of Bernoulli's apparatus. *Instrumentation Measure Métrologie*, 22(5): 201-207. <https://doi.org/10.18280/i2m.220503>
- [20] Shah, R.K., London, A.L. (1978). *Laminar Flow Forced Convection in Ducts*. Academic press. Oxford Academic Press, New York, USA, Supplement 1 to advances heat transfer.
- [21] Al-Nakeeb, Q.A., Fayyadh, E.M., Hasan, M.R. (2021). Experimental investigation of sub-cooled flow boiling heat transfer in single rectangular metallic micro-channel. *IOP Conference Series: Materials Science and Engineering*, 1094: 012056. <https://doi.org/10.1088/1757-899X/1094/1/012056>
- [22] Mohammed, S.A., Fayyadh, E.M. (2020). Experimental study on heat transfer and flow characteristics in subcooled flow boiling in a microchannel. *Journal of Engineering*, 26(9): 173-190. <https://doi.org/10.31026/j.eng.2020.09.12>
- [23] Husseina, H.Q., Fayyadh, E.M., Hasan, M.R. (2024). Investigating the effect of electroplated coatings on single-phase fluid flow and heat transfer in microchannel. *Engineering and Technology Journal*, 42(1): 117-134. <https://doi.org/10.30684/etj.2023.141194.1487>
- [24] Mirmanto, D.B., Kenning, D., Lewis, J., Karayiannis, T. (2012). Pressure drop and heat transfer characteristics for single-phase developing flow of water in rectangular microchannels. *Journal of Physics: Conference Series*, 395: 012085. <https://doi.org/10.1088/1742-6596/395/1/012085>
- [25] Al-Mumen, H. (2023). Design and evaluation of a spider web-like single-axis Micro-Electro-Mechanical Systems accelerometer with high sensitivity and fast response. *Instrumentation Measure Métrologie*, 22(5): 209-214. <https://doi.org/10.18280/i2m.220504>

NOMENCLATURE

A	Area m ²
C _p	Specific heat at constant pressure J/kg K
D	diameter m
f	Fanning friction factor
g	Gravitational acceleration m/s ²
G	Mass flux kg/m ² s
h	Heat transfer coefficient W/m ² K
H	depth m
i	Enthalpy J/kg
I	Current A
k	Thermal conductivity W/m K
L	length m
<i>m</i>	Mass flow rate kg/s
P	Power Watt
P	Pressure Pa
q"	Heat flux W/m ²
Q	Heat W
th	Distance between thermocouple location and channel base m
T	Temperature °C
V	Voltage V
V	velocity m/s
W	width m
Z	Distance measured from inlet channel m
Re	Reynolds number
Pr	Prandtl number
k	thermal conductivity, W.m ⁻¹ . K ⁻¹
Nu	local Nusselt number along the heat source

Greek symbols

ρ	Density kg/m ³
β	Aspect ratio
Δ	Difference, Drop (K, Pa)
μ	Viscosity kg/m s

Subscripts

a	Ambient
app	Apparent
Avg.	Average
b	base
ch	Channel
cu	Copper
br	Brass
f	fluid
FD	Fully developed flow
e	Exit
g	Gas, vapour
h	hydraulic
hy	hydrodynamically developing flow
i	Inlet
l	Liquid
lg	Vaporization
loss	loss
m	Measured
o	Outlet
sat	Saturation
sp	Single-phase
sc	Sudden contraction
se	Sudden expansion